Astron. Astrophys. 335, 69–84 (1998)

ASTRONOMY AND ASTROPHYSICS

Close projected QSO-Galaxy associations: are they real?⋆

J.-F. Claeskens⋆⋆ and J. Surdej⋆⋆⋆

Institut d'Astrophysique et de Géophysique, Université de Liège, Avenue de Cointe 5, B-4000 Liège, Belgium

Received 29 December 1997 / Accepted 16 March 1998

Abstract. The present status of close projected associations between high redshift quasars and foreground galaxies is reviewed in the framework of gravitational lensing, adopting both an observational and a theoretical approach. The Non Singular Isothermal Spherical lens model (Hinshaw & Krauss 1987) is used. We confirm that a stronger overdensity q of *bright* galaxies is expected at *small* projected angular separations ($\leq 3''$) from high redshift and bright (thus highly luminous) quasars (HLQs). The effects of a non singular galactic core radius and/or microlensing only slightly enhance this expected overdensity. The predictions reproduce pretty well the scarce observations which are presently available, with the exception of two rather high overdensities previously claimed in the literature (e.g. $q = 2.9$ for $\theta \leq 6''$, Webster & Hewett 1990). Uncontrolled morphological selections may affect these controversial results so that additional unbiased observations are badly needed before rejecting gravitational lensing as the mechanism to produce the observed close angular QSO-galaxy associations.

We describe three new selected and bias-free samples consisting of a total of 219 different HLQs. Although an apparent overdensity is detected in two of them, these galaxy excesses are found to be statistically not significant.

Firm confirmation of the reality of close projected QSO-Galaxy associations is hampered by small number statistics: the expected and observed absolute numbers of such QSO-galaxy associations are still presently found to be very small. Therefore, the corresponding error bars are quite large. We conclude that the best observational strategy to *significantly* detect (at 3σ) an overdensity of galaxies near HLQs is to observe about 1500 HLQs ($M_V \sim -29$) down to a limiting magnitude $R_{lim} \sim 23$. Future automated surveys may provide us with such a large and unbiased database.

In conclusions, we find that the lensing-induced correlation between galaxies and HLQs at small angular separations consists of a very interesting but weak effect, much less sensitive to cosmological or astrophysical parameters than the number of multiply imaged sources expected within a sample of HLQs.

Key words: quasars: general – galaxies: statistics – cosmology: gravitational lensing

1. Introduction

Close projected associations between quasars and galaxies have already been the subject of controversial studies in the past. The very low *a posteriori* probabilities for the existence of such associations have led some astronomers to question the cosmological origin of the quasar redshifts (Arp et al. 1990). However, since galaxies are often found in clusters and since quasars are also subject to galaxy evolution, it was not a surprise to realize that most of the galaxies in association with low redshift quasars ($z < 0.5$) are in fact members of small clusters at the quasar redshifts (Yee and Green 1987).

But the reality and/or the origin of close projected associations between high redshift quasars and (foreground) galaxies are much more controversial. If these associations are real, one (*ad hoc*) explanation could be that high-z QSOs reside in galaxy clusters whose members underwent a strong luminosity evolution (Tyson 1986). Few redshifts have been obtained for these galaxies: they range between $z = 0.1$ and $z = 0.35$ (Webster & Hewett 1990), which is fully compatible with those of foreground field galaxies. Another explanation then became popular: the foreground galaxies gravitationally amplify the flux of the background sources which lie close to their lines-of-sight. In flux limited samples, this introduces a bias responsible for the "artificial" correlation observed between galaxies and distant QSOs (e.g. Webster and Hewett 1990, Fugmann 1990, Magain et al. 1992 and Table 1). Unfortunately, simple modeling of the galaxies show that the expected amplification bias is too low to account for the amplitude of the observed overdensity (Narayan 1989, Kayser & Tribble 1991, Wu et al. 1996). On the other hand, Bartelmann & Schneider (1993) qualitatively showed that the large-scale angular correlation (~ 10 arcmin) reported by Fugmann (1990) could be explained by gravitational lensing due to large scale dark matter inhomogeneities.

Send offprint requests to: Claeskens@astro.ulg.ac.be

⋆ Based on data collected at the European Southern Observatory, La Silla, Chile

⋆⋆ Aspirant du F.N.R.S. (Belgium)

⋆⋆⋆ Directeur de Recherches du F.N.R.S. (Belgium)

Table 1. Small angular scale QSO-galaxy associations: an observational summary. A limiting magnitude $R_{lim} \sim 22$ is estimated for the galaxies. First column indicates the reference; second column gives the number N_{obs} of observed QSOs in the sample; third column lists the selection criteria to search for associations (θ = angular distance from the QSO, b_j, v, r = blue, visual or red QSO magnitudes; M_V = absolute visual QSO magnitude; z = QSO redshift); column no 4 indicates the analysis method; last column gives the derived overdensity q_{obs}.

Reference	N_{obs}	Selection criteria	Method	q_{obs}
Webster et al. 1988	285	$\theta < 6''\,\vert\, b_j < 18.7\,\vert\, 0.5 < z < 3.2$	Optical Search & counts of QSOs	4.4±0.6
Webster & Hewett 1990	630	$\theta < 6''\,\vert\, b_j < 18.7\,\vert\, 0.5 < z < 3.2$	Optical Search for QSOs & galaxy counts	2.9±0.4
Magain et al. 1990	83	$3'' < \theta < 13''\,\vert\, M_V < -28\,\vert\, z > 1$	Selected HLQs & visual counts	1.3
Drinkwater et al. 1991	44	$16 < v < 17.5\,\vert\, 1 < z < 2.5$	Selected bright QSOs & NNG+KS[a]analysis	Significant
Drinkwater et al. 1992	68	$\theta < 15''\,\vert\, v < 18.5\,\vert\, 1 < z < 2.5$	Selected bright QSOs & NNG +KS analysis	Significant
Magain et al. 1992	153	$\theta < 3''\,\vert\, v < 18.5\,\vert\, M_V < -28$	Selected HLQs & visual counts + PSF subtraction	3.5
Crampton et al. 1992	101	$\theta < 6''\,\vert\, v < 18.5\,\vert\, M_V < -28$	Selected HLQs & automated counts + PSF subtraction	1.4±0.4
Yee et al. 1992	94	$\theta < 2''/6''/15''\,\vert\, v < 19\,\vert\, z > 1.5$	Selected HLQs & automated counts + CP[b] analysis	1.0±0.2
Kedziora-Chudczer & Jauncey 1993	181	$6'' < \theta < 90''\,\vert\, v < 18.5\,\vert\, z > 0.65$	Selected PKS QSOs & automated counts	~ 1.0
Van Drom et al. 1993	135	$3'' < \theta < 13''\,\vert\, M_V < -28\,\vert\, z > 1$ $\theta < 3''\,\vert\, M_V < -28\,\vert\, z > 1$	Selected HLQs & visual counts + Student test	1.4± 0.1 2.8± 0.7
Thomas et al. 1995	64	$15.5 < r < 18.5\,\vert\, z > 1$	Selected bright QSOs & NNG +Binomial stat.	1.7 ± 0.4
This work 1998	219	$1'' < \theta < 20''\,\vert\, M_V < -27.5\,\vert\, z > 1$	Selected HLQs & automated counts + PSF subtraction	Not significant

[a] NNG+KS = Nearest Neighbour Galaxy and Kolmogorov-Smirnov statistical test
[b] CP = Contour Plot

The reality of all the close associations is questionable because of the large dispersion in the observational results coming from the different groups (see Table 1). Positive results seem to be correlated with the method of analysis: visual counts lead more often to overdensities.

In this paper, we concentrate on the small angular scale associations, and we argue that the apparent discrepancy between the observations cannot be explained by the heterogeneity of the samples under study, but do only reflect the large error bars *expected* with such small samples as well as bias selection effects. This may simply be understood since the QSO-galaxy association phenomenon is a weak lensing effect, which can easily be contaminated by unrelated nearby objects. Moreover, the overdensity measurement, like every correlation detection, is very sensitive to the adopted normalization, to the statistical noise and to uncontrolled biases which can affect the original samples. The high observed overdensities cannot be reproduced with a single lens model, except for unrealistically large values of the galactic core radius. We finally present a new analysis of part of the Van Drom et al. (1993) sample and of two new bias-free luminosity selected QSO samples which show *no significant* overdensity.

In Sect. 2, we review the basic formalism of lensing in the framework of the (Non Singular) Isothermal Spherical (IS) lens model and, considering the populations of elliptical, lenticular, spiral and irregular galaxies, we derive the expression for the expected overdensity of galaxies around *selected* quasars[1]. In Sect. 3, we define the best strategy to search for associations and we explore the influences due to core radius, microlensing and galaxy correlation. In Sect. 4, we derive the minimum number of quasar observations needed to significantly detect the lensing signature (amplification bias) in apparent QSO-galaxy associations. In Sect. 5, we present three new searches for associations among Highly Luminous Quasars and discuss our results by comparing them with theoretical predictions and other reported observations. We then look at future results expected from automated surveys; we focus on the Liquid Mirror Telescope project and on "all sky" surveys in Sect. 6. Conclusions form the last section.

Throughout this paper, we adopt the flat Einstein - de Sitter universe model ($\Omega_o = 1, \lambda_o = 0$), with $H_o = 100h$ km/s/Mpc.

[1] None of our QSO samples is complete.

Table 2. Adopted values for the Schechter parameters.

Type	$\Phi_{o,i}$ (h^3 Mpc^{-3})	$M^*_{b_j,i}$ ($h=1$)	α_i
E	0.003	-19.7	-0.85
S0	0.007	-19.2	-0.94
Sb	0.015	-19.2	-0.81
Im	0.006	-19.2	-1.87

2. Formalism of gravitational lensing

2.1. The lensing galaxies

The lenses are assumed to be individual field galaxies, described by a uniform comoving density. Pure luminosity evolution is included by means of the K+evolutive corrections provided by Pozzetti et al. (1996). Therefore, their proper spatial density can be drawn from the four ($i = 1, 4$) local Schechter luminosity functions

$$\Phi_i(z, L)dLdz = \Phi_{o,i}(1+z)^3 \left(\frac{L}{L_i^*}\right)^{\alpha_i} \mathrm{e}^{-(L/L_i^*)} \frac{dL}{L_i^*} dz \qquad (1)$$

corresponding to the elliptical (E), lenticular (S0), spiral (Sb) and irregular (Im) types. The adopted Schechter parameters mainly come from the CfA redshift survey (Marzke et al. 1994). The high normalization we choose for the E+S0+Sb reproduces well the IR counts without evolution (see e.g. Pozzetti et al. 1996). The normalization of the irregulars is taken from Marzke et al. (1994). Adopting a mixing ratio of 12% for the ellipticals (Fukugita & Turner 1991), their abolute normalization turns out to be 10 times smaller than in Schneider (1989). The various adopted luminosity function parameters are listed in Table 2. In the R and K bands, the luminosity functions are translated by the respective local colours of the galaxy types (see Table 3).

In order to describe the gravitational influence of the galaxies, we use the softened isothermal spherical (IS) model (Hinshaw & Krauss, 1987; see Sect. 2.3). This is a very good approximation for the lensing effects of the ellipticals (E/S0) and of the spiral dark haloes[2]. This model can either produce 1, 2 or 3 images, depending on whether the source position lies inside, on, or outside the radial caustic. The third image is generally demagnified.

The irregular galaxies do not significantly contribute to lensing, but they must be taken into account in the simulations, because they may contaminate the observed counts. The Tully-Fisher (1977) (resp. the Faber-Jackson 1976) observed relation between the luminosity L and the velocity dispersion σ of the spiral (resp. elliptical) galaxies is assumed to be valid throughout the optical to near infrared wavelengths:

$$\frac{\sigma}{\sigma_i^*} = \left(\frac{L}{L_i^*}\right)^{1/\gamma_i}, \qquad (2)$$

[2] Including ellipticity in the lens model would only affect the expected galaxy overdensity very close to the quasar, where multiple imaging occurs. This effect could not be distinguished from the observations which are too scarce. Conclusions of the present paper would not be modified.

Table 3. Adopted galaxy colours $b_j - K$ (Glazebrook et al. 1994), $b_j - R$ (Metcalfe et al. 1991) and velocity dispersions for the various types of local galaxies (see text).

Type	$b_j - K$	$b_j - R$	σ_i^* (km/s)
E	4.0	1.5	240
S0	4.0	1.5	200
Sb	3.3	1.3	135
Im	2.2	0.7	100

where $\gamma_i = 4$ for E/S0 galaxies and $\gamma_i = 2.6$ for Sb/Im types (but see Peletier & Willner 1993). The σ_i^* parameters are coherently computed, following the procedure in Fukugita & Turner (1991) for the values of the absolute magnitudes $M^*_{b_j,i}$ listed in Table 2. For the irregulars, a fiducial value of $\sigma_i^* = 100$ km/s is adopted. The results are listed in Table 3.

The core radius r_c of ellipticals scales with luminosity (Kochanek 1996):

$$\frac{r_c}{r_c^*} = \left(\frac{L}{L^*}\right)^{1.2}. \qquad (3)$$

In our study, r_c^* is viewed as a free parameter since we seek its influence on the predicted galaxy overdensities. For simplicity, r_c^* is assumed to be identical for each galaxy type.

2.2. Theoretical overdensity

The expected theoretical overdensity q_i of type i galaxies, with luminosity $\mathcal{L} = L/L_i^*$ at redshift z and angular separation between θ and $\theta + \Delta\theta$, from a *selected* quasar with magnitude b_q at redshift z_q is:

$$q_i(z_q, b_q; z, \mathcal{L}, \theta, \Delta\theta) = \frac{\Sigma_{i,GL}(z_q, b_q; z, \mathcal{L}, \theta, \Delta\theta)}{\Sigma_{NL}(z, \theta, \Delta\theta)}. \qquad (4)$$

Σ_{NL} (resp. Σ_{GL}) is the geometrical cross-section at redshift z in the non-lensing (resp. lensing) situation, i.e. when we search for galaxies around a random point on the sky (resp. around a background QSO). Thus, Σ_{NL} is simply the surface of an angular ring projected at redshift z; it does only depend on the galaxy redshift z through the galaxy angular distance $D_{od}(z)$:

$$\Sigma_{NL} = \pi D_{od}^2(z)[(\theta + \Delta\theta)^2 - \theta^2]\,. \qquad (5)$$

The computation of $\Sigma_{i,GL}$ is more complex. It must include the effects of both the field reduction F and light amplification A, due to the gravitational lensing (GL) phenomenon. Let us first consider the field reduction effect.

Since multiple imaging can occur when a quasar is lensed, we shall only consider in the following the associations between the *brightest* lensed QSO image[3] and the foreground galaxy. We note here that from the cross-section geometrical point of view in flux limited samples, it is equivalent to search for galaxies around selected QSOs or for QSOs around galaxies. The source

[3] Usually, image 1 is the brightest; when the source lies close to the radial caustic, image 2 becomes the brightest one.

plane of the quasar is the physical plane for computing cross-sections, but our association-criterium is defined in the image plane. The field reduction comes from the geometrical mapping of the source plane ($\boldsymbol{\theta_s}$) onto the image plane ($\boldsymbol{\theta}$), and is described by the jacobian of the (2D) lens equation:

$$\boldsymbol{\theta_s} = \boldsymbol{\theta} - \frac{D_{ds}}{D_{os}}\boldsymbol{\alpha}(\boldsymbol{\theta}), \tag{6}$$

where $\boldsymbol{\alpha}$ is the deflection angle, $\boldsymbol{\theta_s}$ is the source position with respect to the galaxy and the D_{ij} are the cosmological angular distances between the *d*eflector, the *o*bserver and the *s*ource. The inverted lens equation has generally more than one solution, thus the change of variables defined in Eq. (6) is valid when considering only one of the lensed images. Since the specific intensity is preserved by lensing (Etherington 1933), the amplification of the considered image is the inverse of the jacobian of the transformation (6). Therefore, if we define θ_1 as the position of the brightest lensed QSO image we are interested in, the field reduction is:

$$F = \tfrac{1}{A(\theta_1)},$$

and one can then write an intermediate result for $\Sigma_{i,GL}$:

$$\Sigma_{i,GL} = 2\pi D_{od}^2(z) \int_{\theta}^{\theta+\Delta\theta} \frac{\theta_1 d\theta_1}{A(\theta_1)}. \tag{7}$$

But when a QSO is lensed into one or multiple unresolved subimages, its flux is increased by a factor A_{tot}, which is the sum over all individual image amplifications. Therefore, lensed QSOs belong to an intrinsically fainter population of quasars. Because faint quasars are much more numerous than bright ones, the chance to get a QSO close to a galaxy is increased by the factor $C(b_q) = N_Q(b_q + 2.5\log A_{tot})/N_Q(b_q)$, where $N_Q(b_q)$ is the observed QSO number counts on the sky (assumed to be unaffected by lensing). The corrected expression for $\Sigma_{i,GL}$ then becomes:

$$\Sigma_{i,GL} = \frac{2\pi D_{od}^2(z)}{N_Q(b_q)} \int_{\theta}^{\theta+\Delta\theta} N_Q(b_q + 2.5\log A_{tot}(\theta_1))\,\tfrac{\theta_1 d\theta_1}{A(\theta_1)}, \tag{8}$$

where

$$\begin{cases} A_{tot}(\theta_1) = A(\theta_1) + |A(\theta_2(\theta_1))| + |A(\theta_3(\theta_1))| & \text{(3 images)} \\ A_{tot}(\theta_1) = A(\theta_1) & \text{(1 image)} \end{cases},$$

$\theta_2(\theta_1)$ (resp. $\theta_3(\theta_1)$) representing the position of image 2 (resp. 3) as a function of the position of image 1. A_{tot} and A also depend on z_q, z, and $\mathcal{L}$ through the lens model (see Sect. 2.3).

Narayan (1989) provides a double power-law fit[4] to the observed QSO number counts measured by Boyle et al. (1988):

$$N_Q(b_q) \propto \begin{cases} 10^{\alpha(b_q-19.15)} & \text{with } \alpha = 0.86 \ \& \ b_q < 19.15 \\ 10^{\beta(b_q-19.15)} & \text{with } \beta = 0.28 \ \& \ b_q \geq 19.15 \end{cases}. \tag{9}$$

With Eqs. (5) and (8), Eq. (4) simply transforms into[5] :

$$q_i(z_q, b_q; z, \mathcal{L}, \theta, \Delta\theta) = \frac{2\int_{\theta}^{\theta+\Delta\theta} N_Q(b_q+2.5\log A_{tot}(\theta_1))\,\frac{\theta_1}{A(\theta_1)}d\theta_1}{\frac{1}{[(\theta+\Delta\theta)^2-\theta^2]}\,N_Q(b_q)}. \tag{10}$$

Summing over all galaxy types and integrating over the galaxy redshift and the observable luminosities, we get the expected observed overdensity of galaxies close to the selected quasar:

$$q_{obs}(z_q, b_q; \theta, \Delta\theta) = \frac{\sum_{i=1}^{4}\int_0^{z_q}\int_{\mathcal{L}_{i,inf}}^{\infty} q_i(z_q,b_q;z,\mathcal{L},\theta,\Delta\theta)\,n_i(z,\mathcal{L})\,d\mathcal{L}dz}{\sum_{i=1}^{4}\int_0^{z_q}\int_{\mathcal{L}_{i,inf}}^{\infty} n_i(z,\mathcal{L})\,d\mathcal{L}dz}. \tag{11}$$

$n_i(z,\mathcal{L})$ represents the number of type i galaxies with luminosity $\mathcal{L}$ and redshift in the interval z, $z+dz$:

$$n_i(z,\mathcal{L}) = \Sigma_{NL}\frac{cdt}{dz}\Phi_i(\mathcal{L}, z), \tag{12}$$

with

$$\frac{dt}{dz} = \frac{1}{H_o(1+z)} \ \cdot \ 1/\sqrt{(1+z)^3\Omega_o - (1+z)^2(\Omega_o+\lambda_o-1)+\lambda_o}. \tag{13}$$

$\mathcal{L}_{i,inf}$ is the luminosity of the faintest type i galaxy that we can detect, given the luminosity distance D_L, the limiting magnitude m_{lim} for the galaxy detection and the K + evolutive corrections $Ke_i(z)$ in the selected filter (Pozzetti et al. 1996):

$$\begin{aligned} \mathcal{L}_{i,inf} &= 10^{0.4(M_i^*-M_{sup})}, \\ M_i^* - M_{sup} &= M_{i,h=1}^* + Ke_i(z) + 5\log f(z,\Omega_o,\lambda_o) \\ &\quad -m_{lim} + 42.386, \\ f(z,\Omega_o,\lambda_o) &= \tfrac{H_o}{c} D_L(z,\Omega_o,\lambda_o). \end{aligned} \tag{14}$$

It is important to note that $q_{obs}(z_q, b_q; \theta, \Delta\theta)$ does finally not depend on the adopted value for H_o.

[4] The change of slope with magnitude is responsible for the magnitude dependence of the correcting factor $C(b_q)$: *selecting* bright QSOs enhances the chance to discover multiply imaged sources or close galaxy-associations. This is the so-called amplification bias (Press & Gunn 1973, Turner, Ostriker & Gott 1984, Fukugita & Turner 1991). A single power-law fit (Hawkins & Véron 1995) would produce a constant correction factor.

[5] Eq. (10) generalises the expression $q = N_Q(< b_q + 2.5\log A)/(N_Q(< b_q)A)$ (Narayan 1989), where $N_Q(< b)$ is the integrated QSO number counts, and which can only be used if the lens produces a single image, assuming that the quasar survey is complete down to the magnitude b_q. In our *selected* samples, Eq. (10) has to be evaluated for each individual quasar.

2.3. The lensing model

In this section, we explore some of the analytical properties of the non singular isothermal spherical lens model (Hinshaw & Krauss 1987). The existence of analytical solutions allows one to include the effect of the radial caustic, which enhances the amplification of single images. The matter density distribution for this model is isothermal far from the center, but converges to a finite value in the core, characterized by the length r_c. The deflection angle writes:

$$\alpha = \frac{4\pi\sigma^2}{c^2}\left(\frac{\sqrt{\xi^2+\xi_c^2}-\xi_c}{\xi}\right), \tag{15}$$

where $\xi = \theta/\theta_E$, $\xi_c = r_c/(D_{od}\theta_E)$, and θ_E is the Einstein angular radius for this lens model. The separation between images 1 & 2 is $\Delta\xi_{12} \sim 2\sqrt{1-2\xi_c}$. This latter relation holds exactly when the source and the lens are coaligned, but it is nearly independent on the source position (see Eq. (17)). Adding a core radius removes the density singularity and decreases the central velocity dispersion. However, in order to reproduce the *observed* stellar velocity dispersion or angular separation between the lensed images, the dark matter velocity dispersion σ should be increased (Kochanek 1996). The angular separation between the lensed images is preserved by means of the following rescaling:

$$\sigma = \sigma_{SIS}\sqrt{\xi_{c,SIS}+\sqrt{\xi_{c,SIS}^2+1}}, \tag{16}$$

where $\xi_{c,SIS} = r_c/(D_{od}\theta_{E,SIS})$ and $\theta_{E,SIS} = \frac{4\pi\sigma_{SIS}^2}{c^2}\frac{D_{ds}}{D_{os}}$ is the angular Einstein radius corresponding to the Singular Isothermal Sphere (SIS) lens model.

The inverted lens equation is cubic and yields the following image positions:

$$\begin{cases} \xi_1 = & 2\rho^{1/3}\cos(\phi/3) + 2\eta/3 \\ \xi_2 = & -\rho^{1/3}\cos(\phi/3) + 2\eta/3 - \sqrt{3}\rho^{1/3}\sin(\phi/3) \\ \xi_3 = & -\rho^{1/3}\cos(\phi/3) + 2\eta/3 + \sqrt{3}\rho^{1/3}\sin(\phi/3), \end{cases} \tag{17}$$

where $\eta = \theta_s/\theta_E$ is the source position and:

$$\begin{cases} \rho = & (-s)^{3/2} \\ \phi = & \arctan\left(\sqrt{-s^3/t^2-1}\right) \end{cases} \text{ and } \begin{cases} s = & \frac{1}{3}\left[2\xi_c - 1 - \frac{\eta^2}{3}\right] \\ t = & \frac{\eta}{3}\left[\xi_c + 1 - \frac{\eta^2}{9}\right] \end{cases}.$$

The solutions (17) are valid when multiple imaging occurs, i.e. when $\xi_c < 1/2$ and the source lies inside the radial caustic, with radius:

$$\eta_R = \sqrt{1 + 5\xi_c - \frac{\xi_c^2}{2} - \frac{1}{2}\sqrt{\xi_c(\xi_c+4)^3}}. \tag{18}$$

Therefore, multiple imaging occurs when the position of image 1, ξ_1, lies in the range $[\xi_{inf}, \xi_{sup}]$, where:

$$\begin{cases} \xi_{inf} = \xi_1(\eta = 0) = \sqrt{1-2\xi_c} \\ \xi_{sup} = \xi_1(\eta = \eta_R) \\ = \frac{2^{2/3}}{3}\left[\eta_R(8\xi_c + 16 + \xi_c^2 + \sqrt{\xi_c(\xi_c+4)^3})\right]^{1/3} + \frac{2\eta_R}{3} \end{cases}.$$

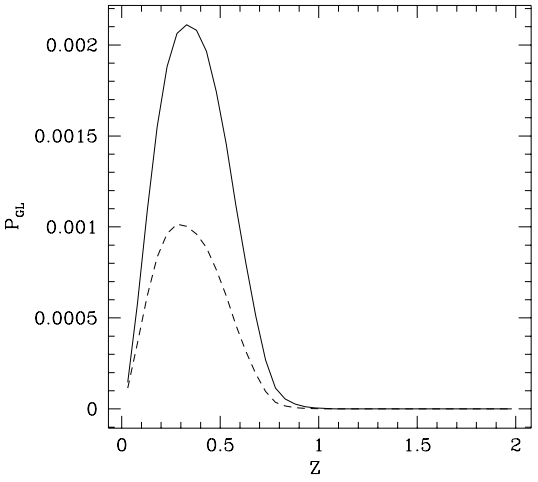

Fig. 1. Expected redshift distributions of observable lensing (solid) and field (dashed) galaxies, for the SIS lens model ($\xi_c = 0$) and default parameter values $z_q = 2$, $b_q = 17$, $\theta \leq 3''$ and $R_{lim} = 21$.

If $\xi_1 = \xi_{sup}$, two of the lensed images are merging on the radial critical line.

The expression for the magnification in the deflector plane is:

$$A(\xi,\xi_c) = \frac{\xi^4\sqrt{\xi^2+\xi_c^2}}{(\xi^2+\xi_c-\sqrt{\xi^2+\xi_c^2})(\xi_c^2+(\xi^2-\xi_c)\sqrt{\xi^2+\xi_c^2})}. \tag{19}$$

Setting $\xi_c = 0$ in the above expressions yields the solutions for the singular isothermal sphere (SIS) lens model (i.e. $\xi_{inf} = 1$, $\xi_{sup} = 2$, $A(\xi) = \xi/(\xi-1)$).

After a change of variables, Eq. (19) can then be inserted into Eq. (10). The positions of image 2 and image 3, corresponding to the position of image 1, are computed using the lens equation (Eq. (6)) and formulae (17).

The total amplification A_{tot} is then known and the expected overdensity of galaxy can be numerically estimated using Eqs. (10) and (11).

3. Signatures of QSO-galaxy associations due to lensing

3.1. Predictions for the SIS lens model

First adopting the simple SIS lens model (i.e. $\xi_c = 0$), we may infer the best observational strategy to identify close projected associations between QSOs and galaxies caused by lensing. We choose the realistic default values of the parameters $z_q = 2$, $b_q = 17$ ($M_v \sim -29$), search radius $\theta \leq 3''$ and limiting magnitude $R_{lim} = 21$ in the R band.

Fig. 1 shows that the expected average redshift of galaxies in associations turns out to be very similar to that of randomly projected normal field galaxies. Therefore, QSO-galaxy associations are not sensitive to the cosmological model (except for their absolute number which remains, though, very small), and will not help in constraining the cosmological parameters. The

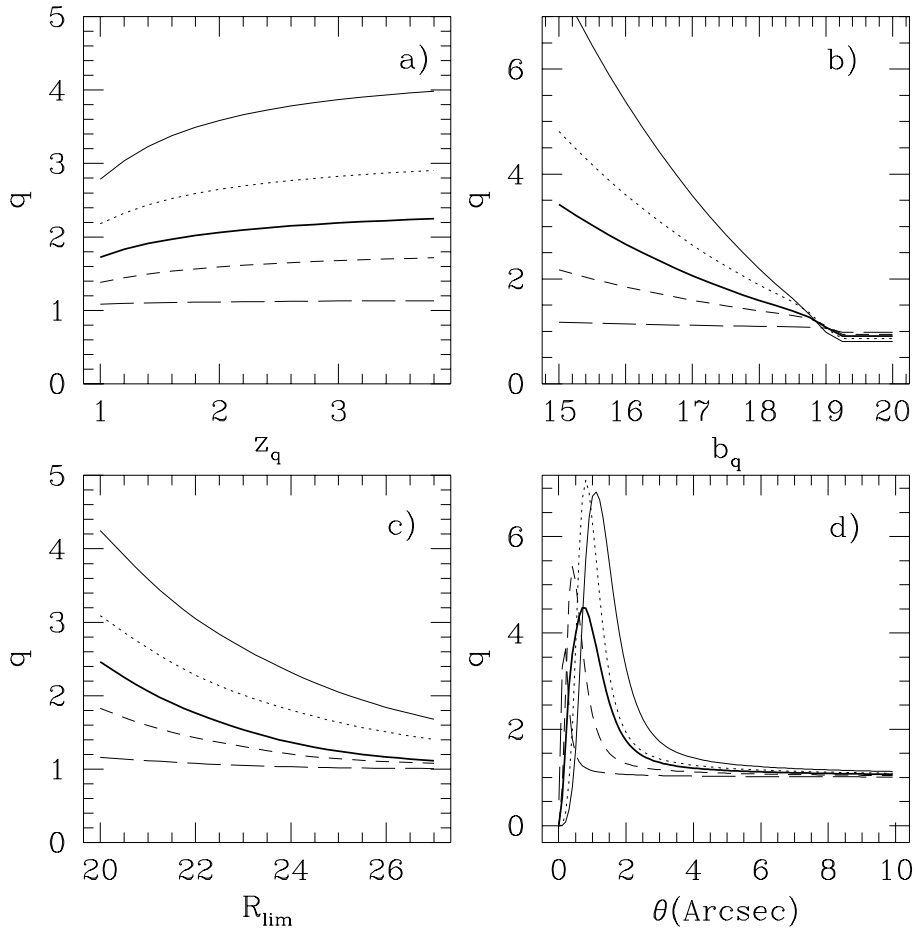

Fig. 2a–d. Theoretical signatures of lensing in QSO-galaxy associations (SIS lens model). The fixed parameters are set to the default values used in Fig. 1. Fig. d) is for a differential ring of radius θ. Thick line: All galaxy types; thin lines: Ellipticals (full), S0 (dotted), Sb (short dash), Im (long dash).

situation is much more favourable when considering the multiply imaged QSO statistics (e.g. Claeskens et al. 1996b), because in that case, we do not need to *detect* the galaxy in order to identify the GL signature.

Fig. 2a-d represent the expected galaxy overdensity around selected quasars as a function of various parameters. As expected, the elliptical galaxies exhibit a stronger signature. Unfortunately, these are not sufficiently numerous and it is also very difficult to observationally distinguish the morphology of faint high redshift galaxies. Therefore, all types of galaxies have to be considered (thick line in Fig. 2). It is straightforward to conclude from this figure that the overdensity is maximal in surveys for bright galaxies within a small vicinity (few arcsec) around high-z and bright (thus, intrinsically luminous) quasars (HLQs). Such samples are by nature incomplete and not deep: they select luminous (massive) galaxies around QSOs for which both the geometrical optical depth for lensing and the amplification bias are high. All samples listed in Table 1 do more or less satisfy these criteria.

3.2. Influence of the core radius

The effects of a non-singular core in the lens model are illustrated in Fig. 3, for $r_c^* = 0.2, 1$ and 2 kpc. As expected from the existence of the radial caustic, the magnification bias is higher than for the case of the singular lens model. As explained in Sect. 2.3, a renormalization is needed to preserve the angular separation between the lensed QSO images (Eq. (16)). Thus, a coherent modeling of the non singular galaxy core shows that its presence *enhances* the overdensity of galaxies in the vicinity of HLQs, while by construction, the typical angular separation is preserved with respect to that predicted with the SIS lens model. This conclusion is opposite to that presented in Zhu et al. (1997), who did not take the renormalization into account.

However, observational constraints on r_c^* from statistics of multiply imaged QSOs (Wallington & Narayan 1993) and galaxy study (Kochanek 1996) imply that r_c^* should be smaller than about 250 h^{-1} pc. This value is corroborated by HST observations of galaxy cores (Crane et al. 1993) . Thus, a realistic value of the core radius parameter leads to a negligible increase of the predicted overdensity relative to that expected with the SIS lens model. For that reason, the simple SIS lens model will be used in all subsequent estimates of the expected galaxy overdensity and for comparison with the observations.

Fig. 3 also shows the effect of increasing the parameter σ^*. As an illustration, it demonstrates that multiplying σ^* by the (controversial) $\sqrt{1.5}$ factor in the SIS model does not help much in increasing the highest expected overdensity. However, at first order, the curve is translated horizontally ($\theta \propto \sigma^{*2}$), resulting

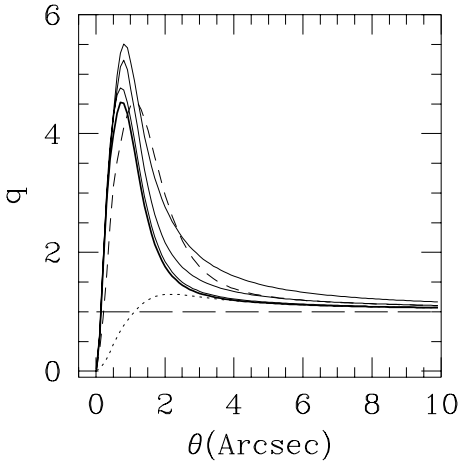

Fig. 3. Influence of the core radius on the differential radial galaxy overdensity profile. Thick line: SIS reference model; thin lines (full, from bottom to top): r_c^* = 0.2, 1 & 2 kpc; dashed line: SIS with $\sigma^*_{DM} = 1.5^{1/2}\sigma^*$; dotted line: SIS model for single imaging only. Default parameters z_q, b_q & R_{lim} have same values as in Fig. 1

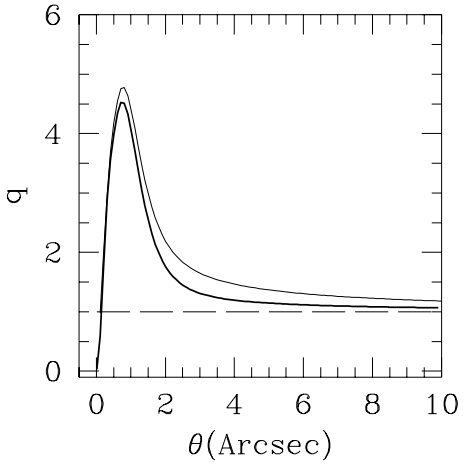

Fig. 4. Influence of microlensing on the radial galaxy overdensity profile. Thick line: smooth SIS reference model; thin line: maximum microlensing by SIS made of compact objects. Default parameters have same values as in Fig. 1.

in a slightly larger predicted overdensity at fixed angular separation (for $\theta > 1''$).

The overdensity expected in the SIS lens model after rejection of multiply imaged QSOs is also displayed in Fig. 3 (dotted line). It shows that most of the expected galaxy overdensity very close ($< 2''$) to the QSOs is correlated with multiply imaged QSOs formed by macro-lensing. However, some of those multiply imaged QSOs will not be detected because of the limited dynamical range.

3.3. Effects due to microlensing

Narayan (1989) has shown in a very elegant way that microlensing may increase the galaxy excess in the vicinity of bright QSOs, but not enough to explain the highest overdensities reported by Webster et al. (1988) or to detect the microlensing signature in close QSO-galaxy associations. In the remainder of this section, we reconsider this effect directly in terms of angular separation (instead of amplification), and for the case of incomplete samples.

A macro image, located at impact parameter θ in the deflector plane may undergo an extra (de-)magnification induced by microlensing due to individual stars or compact objects present along the line-of-sight. As a result, the amplification of the macro image, $A_M(\theta)$, should be replaced by a probability distribution $P(A_\mu, \theta)$ of macro+microlensing amplification A_μ. This distribution depends on the optical depth τ for microlensing and on the macro deflector properties at position θ; it is normalized and if $< A_\mu(\theta) >$ is the mean amplification, the relation $< A_\mu(\theta) >= A_M(\theta)$ must be verified because of flux conservation. Therefore, assuming that microlensing does only[6] affect image 1, Eq. (10) for the differential galaxy overdensity should be replaced with:

$$q_i(z_q, b_q; z, \mathcal{L}, \theta, \Delta\theta) = \tag{20}$$
$$\frac{\int_\theta^{\theta+\Delta\theta} \frac{\theta_1 d\theta_1}{A_M(\theta_1)} \int_{A_o(\theta_1)}^{\infty} \frac{P(A_\mu,\theta_1) N_Q[b_q + 2.5\log(A_{tot}(A_\mu,\theta_1))] dA_\mu}{N_Q(b_q)}}{[(\theta+\Delta\theta)^2 - \theta^2]}$$

where

$$\begin{cases} A_{tot}(A_\mu,\theta_1) = A_\mu + |A_M(\theta_2(\theta_1))| + |A_M(\theta_3(\theta_1))| \text{ or} \\ A_{tot}(A_\mu,\theta_1) = A_\mu \end{cases},$$

depending on whether the number of image(s) is 3 or 1.

There is no general analytical expression for $P(A_\mu, \theta_1)$. Nevertheless, for point-like sources and when the optical depth is small ($\tau \ll 1$), far from any "macro critical line", $P(A_\mu, \theta_1) \sim 2\tau(\theta_1)/A_\mu^3$ for both cases when A_μ is small (but > 1) and $A_\mu \to \infty$ (high amplification regime, Schneider 1987a). Close to the critical line ($A_M \to \infty$), numerical simulations show that $P(A_\mu)$ is nearly a gaussian, centered on A_M (Wambsganss 1992). It thus appears that the function:

$$P(A_\mu, \theta_1) = \frac{2\tau(\theta_1)}{A_\mu^3} + C\delta(A_\mu - A_M(\theta_1))$$

has a correct generic shape (Narayan 1989). Constraint on the probability normalization and flux conservation yield the value of C as well as that of the threshold A_o below which $P(A_\mu, \theta_1) = 0$:

$$\begin{cases} P(A_\mu,\theta_1) = \frac{2\tau(\theta_1)}{A_\mu^3} + (1 - \frac{4\tau}{A_M^2(\theta)})\delta(A_\mu - A_M(\theta_1)), \\ A_o = A_M(\theta)/2. \end{cases} \tag{21}$$

The expression of the optical depth 2τ is given by Schneider (1987a, Eq. 18).

[6] The other images do generally form closer to the galaxy center where the optical depth for microlensing is high. Thus de-amplification frequently occurs on these already fainter images and does not significantly affect the amplification bias.

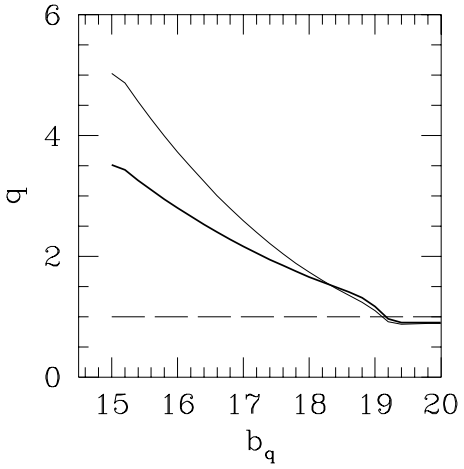

Fig. 5. Influence of microlensing as a function of the QSO blue magnitude. Thick line: smooth SIS reference model; thin line: maximum microlensing by SIS made of compact objects. Default parameters have same values as in Fig. 1.

Within the SIS lens model, the most extreme situation consists in putting all the mass in the form of compact objects. The resulting expected galaxy excess as a function of θ is compared with the case of the smooth model in Fig. 4. Owing to the A_μ^{-3} high amplification tail, microlensing slightly enhances the overdensity of galaxies by a factor which is roughly constant up to $10''$ from the HLQs. But this enhancement factor depends on the QSO apparent magnitude (Fig. 5). Therefore the effect of microlensing on galaxy-QSO associations can only be distinguished in very bright samples ($b_q \leq 16.5$), where it might also help to explain observed overdensities 50% larger than the value predicted by the smooth SIS lens model. At faint magnitudes, the A_μ^{-3} amplification tail does not bring many fainter QSOs above the flux threshold because of the knee in the QSO number counts function (Eq. 9). In our samples, the average QSO blue magnitude is between 17.5 and 18. Therefore the expected mean extra-amplification caused by microlensing is at most 10%, and a very large number of observations would be necessary to significantly (dis)prove the occurence of microlensing from the excess of galaxies closely associated with HLQs. These conclusions are basically the same as those reached by Narayan. On the other hand, if microlensing were really at work, the equivalent width of emission lines in the spectra of QSOs lying close ($\leq 10''$) to galaxies would be smaller than those observed in a sample of isolated quasars (as microlensing mainly affects the continuum emission). Unfortunately, most of the spectra for the galaxy-associated QSOs in our samples have a too low spectral resolution or are simply not available to perform this task. Thus, we cannot directly check for the presence of microlensing in our samples but its influence on galaxy overdensities is expected to be very weak.

3.4. Influence of galaxy-galaxy correlation

Our present model describes the case of uniformly distributed isolated galactic lenses. However, we know that galaxy spatial positions are correlated. This correlation has two consequences: it may "artificially" enhance the observed number of galaxies close to HLQs, and it may modify the lens model (adding mass). Therefore, galaxy-galaxy correlation can only help to reconcile the theoretical predictions with the observations if it is coherently handled. This is not an easy task. However, one can intuitively realize that an isolated lens model constitutes a good approximation in the study of close QSO-galaxy associations. Indeed, the typical Einstein radius of a high redshift L^* galaxy is $R_E \sim 5\ h^{-1}$kpc. On the other hand, using the $(r_o/r)^{1.8}$ correlation function (Groth & Peebles 1977), one can show that the most probable distance between bright galaxies is about $200\ h^{-1}$ kpc (with $n_o = 0.01 h^3 \mathrm{Mpc}^{-3}$), i.e. $\sim 40 R_E$. Thus, in the SIS lens model, a typical light ray passing at $3\ R_E$ from a galaxy undergoes a tiny 3% extra-amplification. This is a negligible quantity, as found by Wu et al. (1996), who modeled the deflector by a SIS plus a matter sheet induced by the neighbouring galaxies (without external shear). Another argument is that the matter density associated with neighbouring correlated galaxies should not modify the statistics of multiply imaged HLQs, for which the mean angular separation between the lensed components has been found in agreement with the single SIS lens model expectations (Surdej et al. 1993, Claeskens et al. 1996b). The matter sheet needed to increase q by 30% would also increase the average angular separation between the lensed images by 12%.

On the other hand, galaxy-galaxy correlation occurs in our observations, but no straightforward statistical test can be performed to disentangle it from random angular projections. The main reason is that our limiting magnitudes are quite bright and the CCD fields are small, resulting in a small number of galaxies per field and a large relative variation of the galaxy number from field to field. Therefore, small scale galaxy-galaxy angular autocorrelation is a source of noise and may contaminate the measured galaxy excess around QSOs.

Since the core radius, microlensing, and galaxy autocorrelation have a negligible influence on the theoretical galaxy overdensity, we adopt in the remainder the smooth SIS lens model.

4. Minimum number of observations

We have seen in Sect. 3.1 that the expected overdensity is maximal for bright galaxies within a few arcsec of HLQs. What is then the best observational strategy to follow?

Since distant quasars have a large geometrical optical depth for lensing and because bright quasars undergo a strong amplification bias, selection of HLQs naturally enhances the probability to find them in association with galaxies. On the other hand, the search for *bright* galaxies in a *restricted* angular vicinity from the quasar (i.e. the most likely lensing galaxies) leads to a

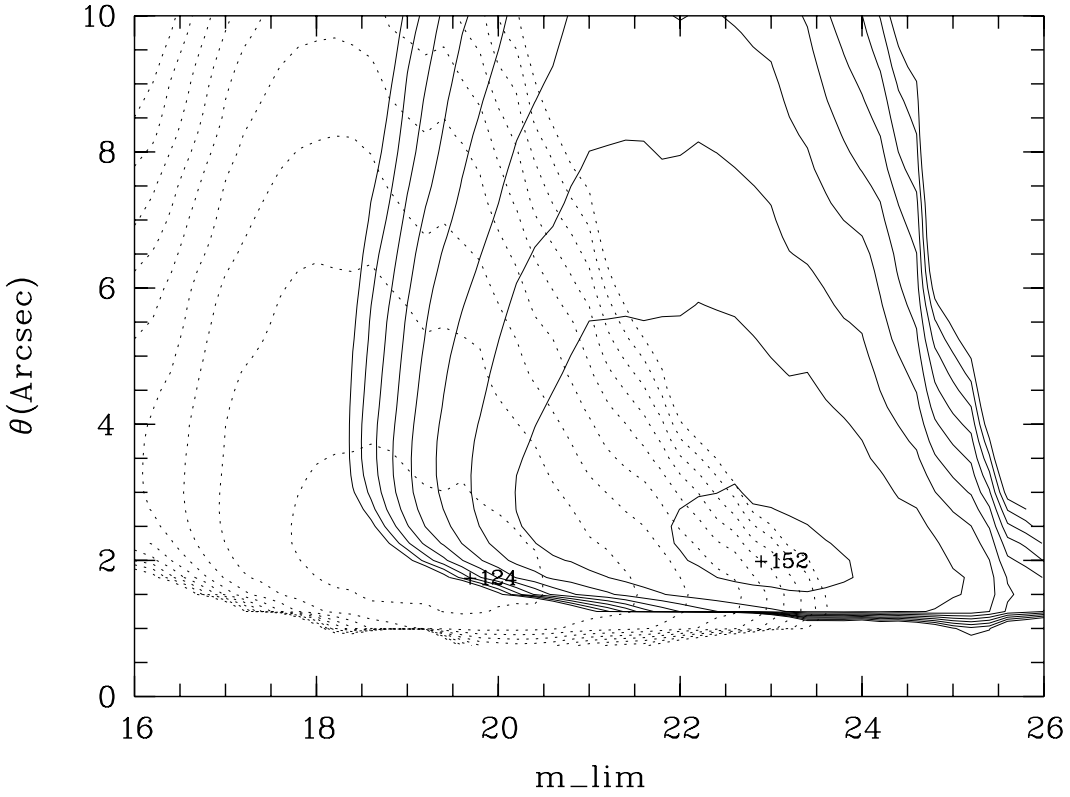

Fig. 6. Minimum requested number N_{min} of HLQs ($M_V \sim -29$) observations to detect a galaxy overdensity at the 1 σ confidence level ($\Omega_o = 1, \lambda_o = 0$). Full lines: R band; dotted lines: K band. First contours are $N_{obs,min} + 50$, then the contour step is 100.

statistical competition between the strength of the lensing signature and the small number of such close associations. Minimizing the number of quasar observations needed to *significantly* detect a galaxy overdensity around QSOs yields a compromise on the most desirable limiting magnitude and on the optimal size for the searching area around the QSOs. The normalization is obtained from the overall galaxy counts, excluding the circular region centered on the QSO and with radius 10″. This normalization also introduces some statistical noise, especially at bright limiting magnitudes and for small fields (like with the IR detectors). We performed numerical Monte-Carlo simulations based on the adopted galaxy luminosity functions and on the SIS lensing model to generate galaxy fields affected or not by lensing (the galaxy autocorrelation was neglected) and to quantitatively derive the minimum number of HLQs needed in order to detect a galaxy overdensity, at the 1 σ confidence level. The fields are assumed to be circular with 1 arcmin (resp. 20 arcsec) radius in the R (resp. K) band. The results are illustrated in Fig. 6 over the (θ, m_{lim}) plane, for the R and K pass-bands. A representative HLQ sample has been chosen with $z_q = 2$ and $b_q = 17$ (i.e. $M_V \sim -29$).

The results displayed in Fig. 6 are much less optimistic than those presented by Schneider (1989). About 150 (resp. 120) $M_V \sim -29$ HLQs have to be observed in the R (resp. K) band in order to detect (at 1σ) the lensing signature. Detection at 3 σ would imply a sample about 9 times larger, i.e. larger than the number of presently known bright QSOs. Although we have not included the microlensing phenomenon (but see Sect. 3.3), we claim that our results are much more realistic, as they reflect the effect of the true galaxy population (Schneider assumes a unique and important population of lensing ellipticals with $\sigma \sim 250$ km/s and no K-correction was made). Our results also include the extra statistical noise due to the normalization. Moreover, the results given in Fig. 6 should be interpreted as lower limits, as they only include the Poissonian noise of a perfect survey. Real surveys might be incomplete with respect to the galaxy counts (influence of the telescope focal length, of the adopted detection/classification method, etc...). These effects are difficult to model. They should further expand the error bars but without changing the measured galaxy overdensity.

All the surveys reported so far in the literature (see Table 1) contain much fewer quasars than statistically required, and this is one of the reasons for the large fluctuations observed between the various analyses. The Webster et al. sample is an exception, but it might be biased as it was first aimed at discovering gravitational lenses (see below).

It was already known that a very large sample of galaxies ($> 10\,000$) was required to significantly detect an overdensity of quasars around galaxies (e.g. Schneider 1987b). In order to detect a galaxy overdensity around quasars, the HLQs sample should be 6 times smaller than the above galaxy sample. This stems from the larger number of galaxies per square degree. But choosing HLQs is a strong selection and the number of

bright and distant QSOs is limited, so that we are also faced with practical difficulties to draw such a sample (see Sect. 6).

The closed contour plots in Fig. 6 betray the competition between the strength of the overdensity and the number of galaxies required to exhibit the phenomenon. For example, about 300 HLQ observations are needed to detect a galaxy overdensity within $3''$ from the QSOs, either for $R_{lim} \leq 20.5$ or $R_{lim} \leq 24$.

From Fig. 6, it is clear that observing in the K band appears to be more efficient to track the lensing signature. This stems from the galaxy colours and K-corrections which favour the detection of high-z massive (lensing) galaxies against faint, blue and local (contaminating) ones. However, because of the much higher sky background in the K band, this better efficiency does not hold anylonger in terms of total observing time. Indeed, based on our observations taken with the ESO/MPI 2.2m telescope in the K' band with the Infrared camera IRAC2-b and in the R band with the direct CCD camera (see Sect. 5.1), we estimate that the integrating time is about 3 times longer to reach $K' = 19$ rather than $R = 23$ (with the same S/N and projected pixel size). Therefore, high angular resolution imaging in the R band pass is the presently most efficient strategy[7]; close inspection of the quasars ($\theta < 2''$) by deconvolution and/or PSF subtraction must also be subsequently performed. The galaxy detection should be complete down to $R_{lim} = 23$.

5. Observations and results

We first present 3 selected HLQ samples, then we describe our technique to count galaxies and, finally, we discuss and compare our results with the theory and other published observations.

5.1. Description of 3 selected HLQ samples

The observed correlation function between QSOs and galaxies is very sensitive to selection effects, especially for small samples in which each association is given much weight. Ideally, the sample should be as free as possible from any uncontrolled selection bias. Since the full Hamburg-ESO QSO catalogue is not yet published (Reimers & Wisotzki 1997), there are presently no complete QSO samples including a large number of bright objects. Therefore HLQ sub-samples have to be taken from heterogeneous compilations (e.g. Véron & Véron 1995). Unfortunately, those compilations reflect the "publication effect", biasing toward "interesting" or "strange" objects. Moreover, most of the observed HLQs have been imaged - and sometimes discovered (Webster et al. 1988, 1990) - while searching for Gravitational Lenses. Pushed by the excitement of the discovery of such rare objects, observers are often unconsciously biasing their sample, based on the peculiar QSO morphology, as first seen on the finding charts. High angular resolution imaging may then reveal some QSO-galaxy associations instead of the suspected multiple quasars. Therefore, a consequence of such a strategy is to artificially enhance the number of QSO-galaxy associations in the sample. We present hereafter 3 "clean" HLQ samples (S1, S2 & S3), whose mean characteristics are given in Table 4. Note that the mean "v" magnitudes are derived from the individual heterogeneous magnitudes as published in the Véron catalogue. However, the meaningful magnitudes needed for the computation of the galaxy overdensity (Eq. 10) are the b magnitudes *at the time of the QSO discoveries*, i.e. when the selection bias was active. Intrinsic flux variations contaminate recent magnitude measurements, while the first ones were often inaccurate and based on photographic material. Faced with this issue, we performed some simulations to test the sensitivity of our results on random and independent uncertainties of half a magnitude on the b flux of each QSO. Thanks to the relatively large number of QSOs, the individual errors cancel each other and the final overdensity is expected to be affected by less than 3%.

We reiterate here that our samples are not complete and that the limiting magnitude does only concern the galaxy detection.

5.1.1. The NTT sample (S1)

This sample corresponds to the S1 sample analysed by Van Drom et al. (1993). Out of the 90 high redshift ($z > 1$) quasars, two were found saturated and one could not be identified. So we are left with 87 quasars. The frames were taken by night assistants during the commissioning period of the New Technology Telescope (NTT) + EFOSC2 ($0.27''$/pixel; 2.3 X 1.4 arcmin^2 field) on La Silla, in August-September 1989. The objects were chosen among the bright ones from the previous edition of the Véron and Véron catalog, according to their visibility at the epoch of observations. These "innocent" observations do not introduce any bias coming from morphological considerations. Short exposure times (2 min. in the R filter) lead to a good image quality (despite the lack of field derotator) and to a rather bright limiting magnitude ($m_{lim} \sim 22$).

5.1.2. The ESO/MPI 2.2m sample (S2)

This sample is extracted from the last observation campaign performed in the context of the ESO Key-Program devoted to the search for Gravitational Lensing, in March 1993. A direct CCD camera ($0.175''$/pixel; 1.8 X 3 arcmin^2 field) was attached to the Cassegrain focus of the ESO/MPI 2.2m telescope (La Silla). The quasars were mainly selected from the Maza et al. (1993) survey, by decreasing order of absolute magnitude (in the observable Right Ascension range). To save telescope time, we relied on the very good telescope pointing and did not use any finding chart. We believe that this kind of "blind" observations should minimize the morphological biases. We have obtained 81 high angular resolution frames. Only 4 frames were rejected due to bad pointing or name-duplication. Rejecting 4 additional QSOs with $z < 1$ (to avoid physical associations with galaxies at the quasar redshift), we are left with 73 HLQs in the S2 sample. The exposure time (5 min in the R filter) was set to avoid the saturation of the bright QSOs. This allowed us to perform subsequent Point Spread Function (PSF) subtractions

[7] Other optical filters are less efficient than the R filter because the CCD sensitivity peaks in the red; in the B band, faint blue galaxies would also contaminate the counts.

Table 4. Mean characteristics of 3 selected HLQ sub-samples (S1, S2 & S3) and the merged sample (M).

Name	Origin	Filter	N_{Obs}	$< z_q >$	$< v_q >$	$< M_{Abs} >$	m_{lim}
S1	NTT + EFOSC2 (8-9/1989)	R	87	2.0	17.6	-27.7	~ 22
S2	ESO/MPI 2.2m + CCD cam. (3/1993)	R	73	2.3	17.6	-28.0	~ 21.5
S3	ESO/MPI 2.2m + IRAC2b (8/1996 & 1/1997)	K	83	2.6	17.4	-28.3	~ 17.5
M	-	-	219	2.3	17.6	-27.9	-

in order to study the immediate QSO surroundings. The limiting R magnitude is around 21.5.

5.1.3. The Near-Infrared sample (S3)

Finally, a new sample of 83 HLQs has been obtained in the near infrared (at 2.2 μm, in the K' band) with the IRAC2-b infrared camera (Lidman et al. 1997) mounted at the Cassegrain focus of the ESO/MPI 2.2m telescope, in August 1996 and January 1997. The B optical lens was used, leading to an apparent pixel size of 0.278″ and a field of view of 71X71 arcsec^2. These HLQs were selected to be the (intrinsically) brightest known ones, and to have on the finding chart a nearby star with in 30″ in order to define an adequate PSF. Unfortunately, due to the blue color of some stars, several QSOs were found to be pretty isolated in K', lacking a proper PSF star companion. These observations are background-limited, and in order not to saturate the detector, telescope offsets and multiple exposures were required. The realignment of the individual frames led to a subsequent reduction of the useful field. The total integration time amounts to 1620 sec per QSO, corresponding to a limiting magnitude of $K' \sim 17.5$.

5.1.4. The merged sample (M)

In order to address a larger QSO sample, we also performed our analysis using the merged sample $M = S1 + S2 + S3$. Due to 24 target duplications (coming from the selection criterium) in the near infrared sample, the finally merged sample contains 219 HLQs. This combined sample is thus heterogeneous but the relevant calculations can anyway be performed (see below).

5.2. Image analysis

Image analysis consisted in two distinct steps: galaxy detection and their counts (S1, S2 and S3 samples), and PSF subtractions (only sample S2) to investigate the close surroundings of the quasars ($< 3''$).

5.2.1. Galaxy counts

The detection and the star/galaxy classification are to be made as clean and objective as possible. Fully automated searches are systematic, but might mis-classify objects, while visual inspection alone may introduce biases in favor of the effect one is looking for. A cross-check is necessary.

The object catalogs for each individual frame have been obtained with "SExtractor", a software for source extractions developed by Bertin & Arnouts (1996). This package has been especially designed to detect and to perform the photometry of non stellar objects. A neural network is used to classify the sources into stars and galaxies. However, the estimator is continuous between 1 (=star) and 0 (=galaxy) and intermediate values correspond to less obvious classification (wrong or uncertain). At low S/N, it is very difficult to assess a threshold between properly classified and unclassified objects. For that reason, we have visually checked each classification. On the oversampled frames of S2, extended faint galaxies were recovered that way. On the other hand, (few) false detections (due to the very low detection threshold) and very faint compact sources have been excluded. Nevertheless, we kept both classifications in our subsequent analysis, to ensure the stability of our results. Due to the compactness of galaxies in the K band, the visual check did not improve over the automated classification.

S2 and S3 observations were made under photometric conditions. Thanks to the archives of the Swiss photometric telescope on La Silla, weather conditions prevailing during the S1 observations could be retrieved, and were found to be photometric as well (Burnet, private communication). Moreover, standard stars in the R band (Graham 1982, Landolt 1992; resp. in the K band, Van der Bliek et al. 1996) were observed every night and the derived CCD zero points of the S1 and S2 (resp. S3) samples were found to be pretty stable during the individual observing runs. Once the zero point is corrected for the atmospheric extinction, the photometry of the galaxies can be performed by SExtractor on each individual frame. The "adaptive aperture magnitudes" computation is based on the "first moment" algorithm introduced by Kron (1980). A 10 pixel wide strip on the edges of each CCD frame has been excluded in order to avoid biaising against extended objects which could fall partially out of the field.

Limiting magnitudes can be estimated in several ways. However, the most stringent limit is dictated by our ability to distinguish between stars and galaxies. Since the individual samples are homogeneous in terms of exposure-time and seeing conditions, the object catalogs of each single frame can be merged to form 3 big catalogs related to each sample. Within those catalogs, the star-galaxy separation limiting magnitude can be estimated by plotting the star/galaxy estimator versus magnitude.

The limiting magnitude is reached when star and galaxy locuses mix up. The estimation of such a limiting magnitude can also be obtained from the comparison between observed and empirical counts (see e.g. Pozzetti et al. (1996) for galaxy counts and Bahcall & Soneira (1980) for galactic star counts). Both methods lead to the same results. The derived average limiting magnitudes listed in Table 4 correspond to a 90% completeness in the star/galaxy observed counts with respect to the expected ones. At the same completeness limit, the limiting magnitudes to only detect a star or a galaxy would be about 1 magnitude fainter. The error on the star-galaxy separation limiting magnitude is estimated to be about 0.5 mag. The mean magnitude error on the photometry at this limiting magnitude is about 0.2 mag.

To avoid biases, it is essential to reject from the analysis all objects fainter than the adopted limiting magnitude of the parent sample.

5.2.2. PSF subtraction

PSF subtraction is aimed at improving the detection of faint objects lying very close (≤ 2 FWHM) from the QSO-targets. Most interestingly, it does also allow us to evaluate the magnitude of even superposed extended objects down to 2 magnitudes fainter than the QSO. This technique works fine only if the data are well sampled (typically FWHM > 3 pixels) and if a high S/N numerical PSF can be defined from the unsaturated stars present in the field. The algorithm has been developed by Remy (1997). Numerical simulations on real data yield a relation between the largest magnitude difference which can be detected (dynamical range) and the angular separation between an extended object and the QSO (Fig. 7).

Because of under-sampling and/or PSF variations across the field in the S1 and S3 samples, PSF subtractions have not been performed for both these samples. In the S2 sample, we were able to build suitable numerical PSFs for 63 frames. Three new results were obtained: the lensed nature of the QSO J03.13 (see Claeskens et al. 1996a & Surdej et al. 1997), a 22 mag galaxy at $2.2''$ from the QSO B30.05 (but subsequently rejected in our study because it is fainter than the limiting magnitude), and one superimposed galaxy on the quasar HE1122−1648.

On the other hand, the S1 and S3 samples have been visually inspected to search for faint objects very close to the QSOs. The S1 sample is highly incomplete for galaxies with $R > 20$ and closer than $2''$ from the bright QSO because of the limited dynamic range (see Fig. 7). Therefore, the galaxy visual counts at $\theta \leq 2''$ are not relevant at a limiting magnitude R_{lim} = 22. In the near-IR sample, the lens galaxy of the double quasar HE1104−1805 has been rediscovered this way. The magnitude and position of the galaxy have been determined with an *a posteriori* PSF subtraction (Remy et al. 1998).

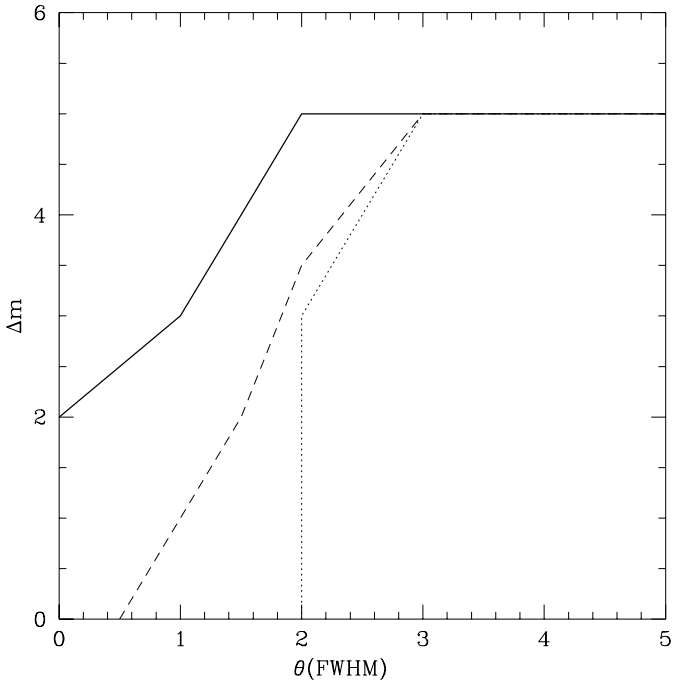

Fig. 7. Dynamical range as a function of the angular separation (in FWHM units) resulting from numerical simulations. PSF analysis, visual detection of anomalous objects or SExtractor photometry+classification of an extended object close to the QSO are only possible within the domains delimited by the full, dashed or dotted lines respectively. The maximum magnitude difference (Δm = 5) is just representative of the CCD dynamical range.

5.3. Results

5.3.1. Overdensities

For a given sample and limiting magnitude, the observed galaxy overdensity inside a circle centered on the HLQs is computed by dividing the number of detected galaxies within that circle by the expected number obtained from the normalization of the overall galaxy counts.

The observed overdensities are compared with theoretical predictions in Fig. 8.

The theoretical curves and error bars in Fig. 8 were computed for each sample from the 1-σ dispersion of the results produced by 1000 Monte Carlo simulations. For each simulation, a random number of galaxies, whose mean value coincides with the observed one in the sample, was distributed in the field according to the theoretical overdensity profile of the sample. This profile was obtained by averaging the overdensity profiles computed with the SIS lens model for each HLQ in the sample (and for the limiting magnitude in Table 4). The simulated fields were then analysed by the same procedure as the observed ones. Therefore, those simulations only include the Poissonian noise due to the galaxy spatial distribution; galaxy auto-correlation and parameter uncertainties were not included. Consequently, the derived theoretical error bars are conservative. Let us note here that the mean absolute number of galaxies expected with our lensing model and the adopted Schechter and color parame-

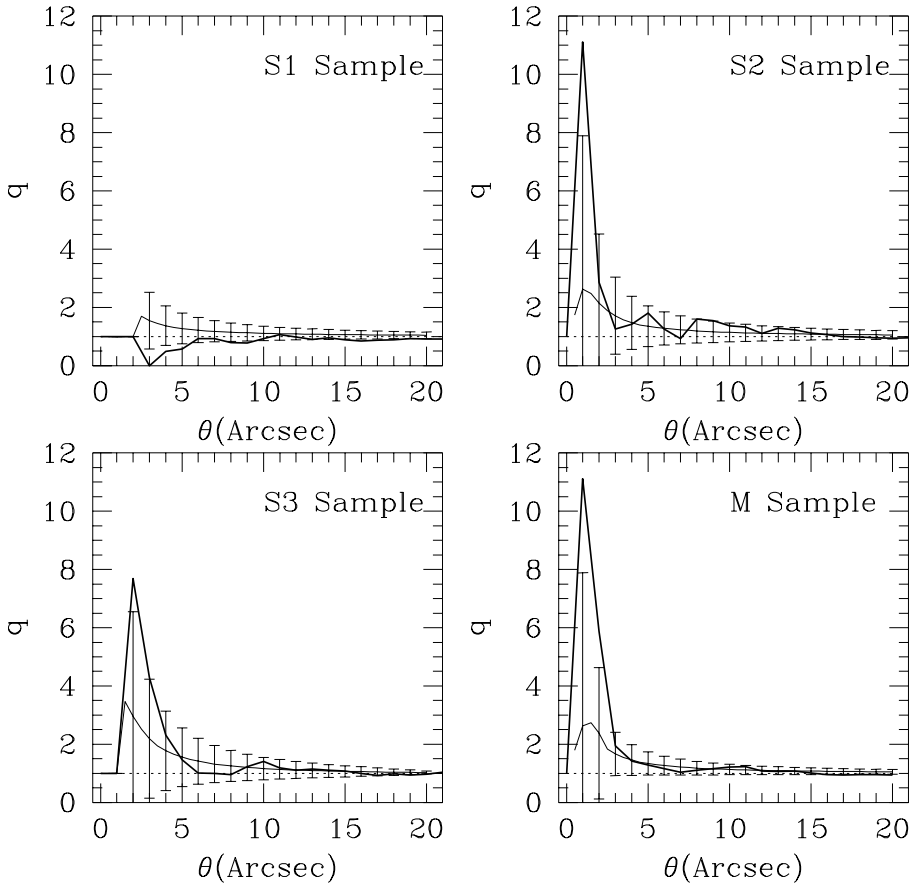

Fig. 8. Overdensities $q(\leq \theta)$ in the different HLQ samples. Thick lines: observations; thin lines and 1σ error bars: results of 1000 Monte Carlo simulations for the SIS lens model and for the derived limiting magnitudes. The dotted lines show the uniform model whose 1σ error bars are much the same as those of the lensing model and have not been represented for clarity.

ters (see Tables 2 & 3) matches pretty well the observed counts. This is a sign of a coherent description and of a good estimation of the limiting magnitudes.

No binning of the data has been done as we look for associations in circular areas around the quasars. Consequently, the error bars shown in Fig. 8 are not mutually independent.

As illustrated in Fig. 8, although a trend for galaxy overdensity is seen in the S2 & S3 samples, no *significant* anomalous number of galaxies in the circular vicinity of HLQs is detected. Indeed, the observed signal never deviates more than 2 σ from the theoretical curve. Note that the strong overdensity peak in the S2 sample is only due to 1 galaxy.

Following our PSF analysis and visual detection very close to the quasar, the simulations for the M sample are obtained from the S2 sample for $\theta < 1''$ (63 HLQs), from the S2+S3 samples for $1'' < \theta < 2''$ (93 HLQs) and from all three samples for $\theta > 2''$ (219 HLQs).

We have performed some statistical tests in order to check the departure of the data from uniformity (the Kolmogorov-Smirnov (KS) test, the "s-test" based on the Nearest-Neighbour Analysis (Thomas et al. 1995) and the Student-Test): none of them was positive. This is not a surprise for the KS test, as it is not well adapted to the kind of statistical fluctuations we are looking for. The "s-test" is not more conclusive due to the small numbers involved. We have also compared the number of galaxies observed in a ring ($3'' < \theta < 13.7''$) centered on the QSOs and the corresponding number detected in a ring centered on a random remote point of the field (cf. Van Drom et al. 1993). The Student Test was not significant. Changing the size of the vicinity or the limiting magnitude does not help. Moreover, significant statistical results should be stable with regard to slight modifications of the selection criteria. Our present new analysis of the NTT data (cf. S1 in Van Drom et al.) proves that the results are unstable. Selecting the QSOs according to their optical or radio flux does not produce any significant change but the reduced sample size leads to even larger error bars.

The large error bars in Fig. 8 are due to small number statistics, and they are fully expected from the moderate size of our samples (see Sect. 4 for the minimum number of observations). They are even so large that the lensing model is statistically compatible with the null hypothesis of uniformity. The lensing model is absolutely not ruled out by our new data. More precisely, our observations are statistically and simultaneously compatible with both a random process and with the lensing model!

5.3.2. Galaxies in associations

In the M sample, the total number of detected galaxies closer than $10''$ from the QSOs amounts to 57 (i.e. 1 galaxy associated with every 3.8 QSOs). The mean magnitude of these galaxies is not significantly different from that of the field galaxies. The

associated QSOs in the S1 & S2 samples are intrinsically 0.2 magnitude brighter than the mean, as expected from the lensing signature. But the associated QSOs observed in the IR sample are on the average fainter than the non associated ones. These differences are not conclusive since they are smaller than the internal dispersion within the samples. The S1 sample seems to suffer from clustering as we count 31 galaxies around 19 QSOs (1 QSO has 4 galaxies and 9 have 2 galaxies). This clustering (at $\sim 10''$) does not show up in Fig. 8 because about half the galaxies are fainter than the limiting magnitude. Clustering cannot be disentangled from GL associations, because of the high frame to frame number count scatter.

5.3.3. General comparison with other surveys

In order to proceed with a general comparison between our results, other published observations and theoretical predictions, we renormalized each data point to a common lensing situation. This reference situation corresponds to the expected overdensity, in the smooth SIS lens model, of galaxies with $R \leq 21$ as a function of their angular distance to an HLQ for which the redshift and the magnitude are $z_q = 2, b_q = 17$, respectively ($M_V \sim -29$)[8]. This differential radial profile is illustrated as the thick curve in Fig. 9. The data points are always obtained by counting galaxies into radial bins. So we binned ours, following the example given by Van Drom et al. (1993), i.e. choosing 3 angular rings with equal areas ($3'' < \theta < 13.7''$, $13.7'' < \theta < 19.1''$, and $19.1'' < \theta < 23.3''$) plus the inner central circle $\theta < 3''$. The abcsissae of the data points are set to the mean radius $< \theta >$ of the bins. The normalization factor applied to any individual data point is given by the ratio of the overdensity in the reference model at $< \theta >$ to that computed with the same SIS lens model and for the corresponding QSO sample, limiting magnitude (and passband), and angular bin. The 1σ error bars have been computed as $\sigma = \sqrt{1/N_{exp}}$ where N_{exp} is the expected number of galaxies assuming that lensing is not active. Webster's sample was defined as the set of 887 quasars with $z > 0.5$ extracted from the LBQS survey (Hewett et al. 1994). The $b_j \sim 21.5$ limiting magnitude was adopted. The results are displayed in Fig. 9.

At first glance, the observed data points follow the theoretical expectation, i.e. the overdensity is increasing very close to the QSO but is not anomalously high. Large error bars (especially for the S3 sample where the absolute number of galaxies is small) prevent to draw definite conclusions. For the same reason, no general strong disagreement is detected. The most deviant data point ($> 3\sigma$) is that of Webster et al. It should be meaningful as it is provided by the largest sample. But this sample, originally aimed at discovering new gravitational lenses, might be subject to a strong selection bias as it is partially based on the QSO candidate morphology. Moreover, some spurious physical

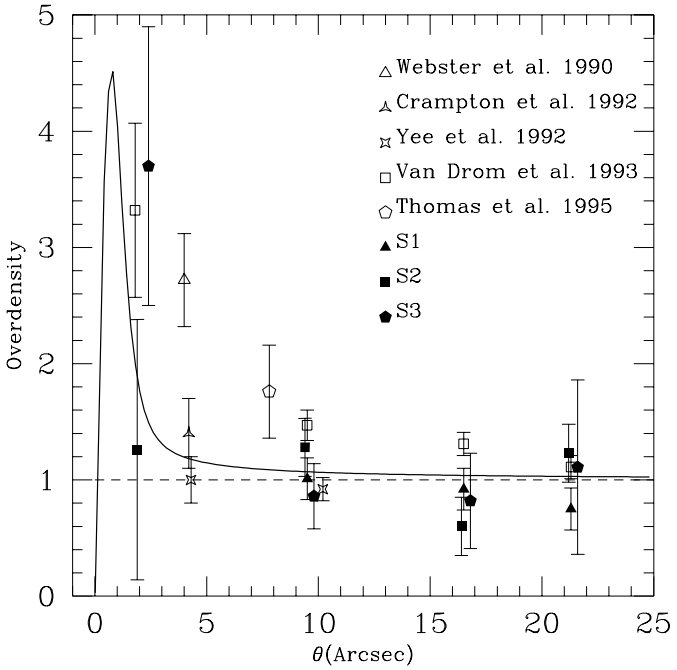

Fig. 9. Compilation of the renormalized observed overdensities of galaxies around HLQs (see Table 1 and text).

associations might be included in the sample because of its lower redshift limit ($z > 0.5$). These are conjectures and should this data point be confirmed by new, bias-controlled, numerous observations, the lensing explanation would be ruled out. Thomas et al.'s data go in the same direction, but less strongly. Their sample is much cleaner with respect to selection biases, but it is also much smaller and their result does not seem to be very stable when altering the galaxy limiting magnitude. The Van Drom et al. results are not statistically compelling, but they are systematically higher than expected. Their sample includes our S1 sample and another one obtained from the first HLQ observations within the ESO Key-program. The latter could be affected by a morphological selection bias as well. However, they also find a statistically significant overdensity between 3 and $13.7''$ in the S1 sample. We cannot reproduce this result, even by including the objects fainter than the star-galaxy separation limiting magnitude. This is the signature of highly unstable results due to small number statistics.

As a conclusion, the bulk of data does not contradict the lensing theory, but highly significant results will be difficult to reach, as a large number of observations is required. This is opposite to the claim by Schneider (1989) that the galaxy overdensity around QSOs is much easier to detect than the QSO overdensity around galaxies, because galaxies are more numerous. They are more numerous, but much contamination comes from the observations of weak and non lensing galaxies while massive and distant lenses may remain undetected. Therefore, QSO-galaxy associations consist of a weak lensing effect. This result also implies that the (non) detection of QSO-galaxy associations is a weak constraint on the claim that lensing might be responsible for a large change in the apparent QSO luminos-

[8] When the reference situation is the SIS lens model *with* microlensing due to compact objects, the results are very similar to those obtained with the smooth SIS lens model, although the corresponding reduced χ^2 value is slightly larger.

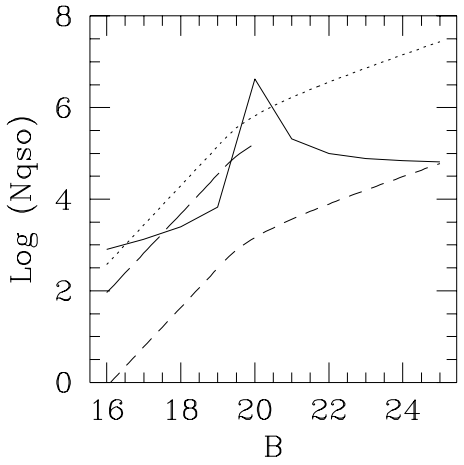

Fig. 10. Total number of QSOs brighter than magnitude B. Full line: required number of QSOs for a 3 σ detection of the galaxy overdensity (for $z_q = 2$ and the optimal parameter values $\theta \leq 3''$ and $R_{lim} = 23$); short dash: expected number of QSOs in the proposed LMT survey; long dash: expected number of QSOs in the Sloan Digital Sky Survey; dots: total number of QSOs over the whole sky.

ity function (as stated by Webster el al. (1988, 1990), but see Schneider 1987c for the effect of a cosmological population of compact objects).

6. Future prospects from automated surveys

Automated surveys are replacing traditional astronomical observations. This "industrial" mode of observation may have the advantage of being systematic, removing "old-fashion" human selection biases and thus providing "clean" samples. As an example, we shall explore the expected output from the Liquid Mirror Telescope (LMT) project (Borra, Ninane & Surdej 1997).

The LMT project consists of a zenithal telescope whose 4m mirror is made of an extremely thin layer of mercury in slow rotation. Therefore, if located for instance at La Silla, this telescope would only have access to a restricted high galactic latitude sky area of about 90 square degrees. About 20 000 QSOs with $B < 24$ should be found in this slice of sky (see Surdej & Claeskens 1997 for more details on the interest of such a survey for GL studies). However, regarding close QSO-galaxy associations, this kind of survey will not allow us to detect a very significant overdensity. Indeed, Fig. 10 shows the required number of QSOs in order to reach a 3 σ detection of the galaxy overdensity in a complete sample as a function of the B limiting magnitude (full line). This number is found to be larger than the total number of QSOs expected within the 1 degree strip LMT survey (short dash), provided the QSO counts can be extrapolated to such faint magnitudes.

In conclusion, a statistically significant detection of QSO-galaxy close associations is very difficult to be achieved. An "all-sky" survey is first required to identify all bright QSOs in the sky. The Sloan Digital Sky Survey (SDSS; Gunn 1995, Loveday 1996) will identify within 5 years all the quasars brighter than $B \sim 20$ in a sky area of 10 000 square degrees at high galactic latitudes. As shown in Fig. 10 (long dash), such a survey is appropriate to detect the galaxy overdensity around QSOs brighter than $B \sim 18-19$. On the other hand, the Hamburg/ESO survey should be available within 3 years (Reimers & Wisotzki 1997). Then, high angular resolution imaging will be needed around approximately 1000 (resp. 10 000) $B < 17$ (resp. $B < 19$) high redshift quasars to get a 3 σ detection of the galaxy overdensity (see Fig. 10).

The required number of quasars peaks at $B \sim 20$. This indicates that no sign of galaxy overdensity is expected in such a flux limited sample: the amplification bias just compensates the field reduction effect. For fainter magnitude thresholds, the field reduction acts alone and a slight galaxy *under*density should become detectable. But on the other hand, if a significant and large (> 2 for $\theta \geq 3''$ and $R_{lim} \sim 21$) galaxy overdensity were detected around faint QSOs in such a clean sample, a physical cause different from lensing should be invoked to explain this anomalous correlation.

7. Conclusions

Adopting the working hypothesis that galaxies may be modeled as isolated Non Singular Isothermal Spheres, that the quasars are point-like and that their observed magnitude-number counts on the sky are intrinsic, we have reviewed in the framework of gravitational lensing the problem of the excess of apparent close associations between high redshift HLQs and foreground galaxies. Our results can be summarized as follows:

1. The expected overdensity of galaxies is maximal for the brightest ones, located at small angular distances ($2 - 3''$) from high redshift and bright QSOs (=HLQs).
2. Microlensing and non singular core radii may increase this expected overdensity.
3. The high observed overdensities (e.g. Webster & Hewett 1990) cannot be reproduced by the theory, even when microlensing and a reasonable size for the core radius are taken into account.
4. The theoretical error bars are large because the expected absolute number of close associations between galaxies and QSOs is small. Therefore the size of the HLQ sample is to be important to get rid of small number statistics. Competition between the amplitude of the expected overdensity and the absolute number of galaxies needed to exhibit the phenomenon leads to the suggestion of an optimal observational strategy. Indeed, in order to detect a galaxy overdensity at the 3σ confidence level, about 1500 HLQs ($M_V < -29$) should be imaged at high angular resolution in the R band to detect galaxies brighter than $R_{lim} = 23$ at angular distances smaller than $2''$. Imaging in the K band is theoretically more efficient as lensing galaxies are preferentially selected, but in practice the R band is more efficient in terms of telescope time.
5. HLQ samples must be carefully checked against any uncontrolled selection bias, especially regarding the morphology. We have presented three new such samples (S1, S2 & S3)

with well defined galaxy detection/classification and limiting magnitude. The observed overdensities are found to be not significant, given the theoretical error bars.

6. The available data coming from different surveys, including ours, have all been normalized to similar observing conditions (regarding the limiting magnitude, the waveband and the HLQ redshift and magnitude) and have been compared with theory. Given their large error bars, those data are compatible with the lensing model as a possible explanation for the observed overdensities. However, the Webster et al. data point is still significantly deviant. This could come from a morphological selection bias in their sample. It needs to be confirmed by additional unbiased observations. If such a confirmation ought to occur, a physical reason different from lensing should be invoked to explain the phenomenon.
7. The Hamburg/ESO survey and future automated all-sky surveys might be promising in providing us with a large and complete HLQ sample. Subsequent high angular resolution imaging of all identified HLQs will be needed to count the galaxies in their immediate angular vicinity. Nevertheless, QSO-galaxy association remains a weak lensing effect. It is not well suited to constrain the cosmological parameters and it is less sensitive to the galaxy physical parameters than the statistical studies of multiply imaged QSOs.

Acknowledgements. We thank Dr. D. Hutsemékers and J.-P. Kneib for their carefull reading and comments on the manuscript. Part of this work has been supported by the SSTC/PRODEX project "HST observations of gravitational lenses" and a belgian FNRS grant.

References

Arp, H.C., Burbidge, G., Hoyle, F., et al., 1990 Nature, 346, 807
Bahcall, J.N., Soneira, R.M., 1980 ApJ S., 44, 73
Bartelmann, M., Schneider, P., 1993 A&A, 268, 1
Bertin, E., Arnouts, S., 1996 A&A S., 117, 393
Borra, H., Ninane, N., Surdej, J., 1997 "The liquid Mirror Telescope (LMT) Project", http://vela.astro.ulg.ac.be/lmt
Boyle, B.J., Shanks, T., Peterson, B.A., 1988 MNRAS, 235, 935
Claeskens, J.-F., Surdej, J., Remy, M., 1996a A&A, 305, L9
Claeskens, J.-F., Jaunsen, A.O., Surdej, J., 1996b, Proceedings IAU 173 "Astrophysical Applications of Gravitational Lensing" , p13-20 (Eds. C.S. Kochanek, J.N. Hewitt)
Crampton D., McClure, R.D., Murray Fletcher, J., 1992 ApJ, 392, 23
Crane, P., Stiavelli, M., King, I.R., Deharveng, J.M. et al., 1993 AJ, 106, 1371
Drinkwater, M.J., Webster, R.L., Thomas, P.A., 1991 ASP Conf. Ser., 21, 317 (Ed. Crampton, D.)
Drinkwater, M.J., Webster, R.L., Thomas, P.A., Millar, D., 1992 Proc. ASA, 10, 8
Etherington, I.M.H., 1933 Phil.Mag., 15, 761
Faber, S.M., Jackson, R.E., 1976 ApJ, 204, 668
Fukugita, M., Turner, E.L., 1991 MNRAS, 253, 99
Fugmann, W., 1990 A&A, 240, 11
Glazebrook, K., Peacock, J.A., Collins, C.A., Miller, L., 1994 MNRAS, 266, 65
Graham, J.A., 1982 PASP, 94, 244
Groth, E.J., Peebles, P.J.E., 1977 ApJ, 217, 385
Gunn, J.E., 1995, Bull. American Astron. Soc.,186, #44.05
Hawkins, M., Véron, P., 1995 MNRAS, 275, 1102
Hewett, P.C., Irwin, M.J., Foltz, C.B. et al., 1994 AJ, 108, 1534
Hinshaw, G., Krauss, L.M., 1987 A&A, 320, 468
Kayser, N., Tribble, P., 1991 ASP Conference Series, 21, 304
Kedziora-Chudczer, L., Jauncey, D.L., 1993 Proc. 31st LIAC, p289
Kochanek, C.S., 1996 IAU Symp. 173, p7 (Eds. Kochanek, C.S., Hewitt, J.N.)
Kron, R.G., 1980 ApJS, 43, 305
Landolt, A.U., 1992 AJ, 104, 340
Lidman, C., Gredel, R., Moneti, A., 1997 IRAC2-b Users Manual v. 1.3 http://www.ls.eso.org/lasilla/Telescopes/2p2T/E2p2M/IRAC2/irac2.html
Loveday, J., 1996 Conference Paper, Recontres De Moriond Workshop
Magain, P., Remy, M., Surdej, J., Swings, J.-P., Smette, A., 1990 Lecture Notes in Physics 360, p 88 (Eds. Mellier, Y., Fort, B., Soucail, G.)
Magain, P., Hutsemékers, D., Surdej, J., Van Drom, E., 1992 Lecture Notes in Physics 406, p 88 (Eds. Kayser, R., Schramm, T., Nieser, L.)
Marzke, R.O., Geller, M.J., Huchra, J.P., 1994 AJ, 108, 437
Maza, J., Ruiz, M.T., González, L.E., Wischnjewsky, M., Antezana, R., 1993 Rev. Mex. Astron. Astrofis., 25, 51
Metcalfe, N., Shanks, T., Fong, R., Jones, L.R., 1991, MNRAS 249, 498
Narayan, R., 1989 ApJ, 339, L53
Peletier, R.F., Willner, S.P., 1993 ApJ, 418, 626
Pozzetti, L., Bruzual, A.G., Zamorani, G., 1996 MNRAS, 281, 953
Press, W.H., Gunn, J.E., 1973, ApJ 185, 397
Reimers, D., Wisotzki, L., 1997 Messenger, 88, 14
Remy, M. 1997 Ph.D. Thesis Liège University
Remy, M., Claeskens, J.-F., Surdej, J., et al. 1998 New Astronomy, in press
Schneider, P., 1987a ApJ, 319, 9
Schneider, P., 1987b A&A, 179, 80
Schneider, P., 1987c A&A, 183, 189
Schneider, P., 1989 A&A, 221, 221
Surdej, J., Claeskens, J.-F., Crampton, D., Filippenko, A.V., Hutsemékers, D. et al.: 1993, AJ 105, 2064
Surdej, J., Claeskens, J.-F., Remy, M. et al. 1997 A&A, 327, L1
Surdej, J., Claeskens, J.-F., 1997 in the proceedings of the Marseille Workshop entitled 'Science with Liquid Mirror Telescopes', april 14-15 1997, Ed. M. Ferrari, in press
Thomas, P.A., Webster, R.L., Drinkwater, M.J., 1995 MNRAS, 273, 1069
Tully, R.B., Fisher, J.R., 1977 A&A, 54, 661
Turner, E.L., Ostriker, J.P., Gott, J.R., 1984, ApJ 284, 1
Tyson, J.A., 1986, AJ 92, 691
Van der Bliek, N. S., Manfroid, J., Bouchet, P., 1996 A&AS 119, 547
Van Drom, E., Surdej, J., Magain, P., et al., 1993 Proc. 31st LIAC, p301
Véron-Cetty, M.-P., Véron, P., 1995, A catalogue of Quasars and Active Nuclei (7th edition), ESO Scientific Report No. 17
Wallington, S., Narayan, R., 1993 ApJ, 403, 517
Wambsganss, J., 1992 ApJ, 386, 19
Webster, R.L., Hewett, P.C., Harding, M.E., Wegner, G.A., 1988 Nat., 336, 358
Webster, R.L., Hewett, P.C., 1990 Lecture Notes in Physics 360, p73 (Eds. Mellier, Y., Fort, B., Soucail, G.)
Wu X.-P., Fang, L.-Z., Zhu, Z.-H., Qin, B., 1996 ApJ, 471, 575
Yee, H.K.C., Green, R.F., 1987 ApJ, 319, 28
Yee, H.K.C., Filippenko, A.V., Tang, D., 1992 Lecture Notes in Physics 406, p83 (Eds. Kayser, R., Schramm, T., Nieser, L.)
Zhu, Z.-H., Wu, X.-P., Fang, L.-Z., 1997 ApJ , 490, 31